fractal and fractional

MDPI

Article

The Effect of Fractional Derivatives on Thermo-Mechanical Interaction in Biological Tissues during Hyperthermia Treatment Using Eigenvalues Approach

Aatef Hobiny [1] and Ibrahim Abbas [1,2,*]

[1] Mathematics Department, Faculty of Science, King Abdulaziz University, Jeddah 21589, Saudi Arabia; ahobany@kau.edu.sa
[2] Mathematics Department, Faculty of Science, Sohag University, Sohag 82524, Egypt
* Correspondence: ibrabbas7@science.sohag.edu.eg

Abstract: This article studies the effects of fractional time derivatives on thermo-mechanical interaction in living tissue during hyperthermia treatment by using the eigenvalues approach. A comprehensive understanding of the heat transfer mechanism and the related thermo-mechanical interactions with the patient's living tissues is crucial for the effective implementation of thermal treatment procedures. The surface of living tissues is traction-free and is exposed to a pulse boundary heat flux that decays exponentially. The Laplace transforms and their associated techniques are applied to the generalized bio-thermo-elastic model, and analytical procedures are then implemented. The eigenvalue approach is utilized to obtain the solution of governing equations. Graphical representations are given for the temperature, the displacement, and the thermal stress results. Afterward, a parametric study was carried out to determine the best method for selecting crucial design parameters that can improve the precision of hyperthermia therapies.

Keywords: living tissue; fractional time derivatives; analytical solutions; thermo-mechanical interactions; Laplace transform; thermal relaxation time

check for updates

Citation: Hobiny, A.; Abbas, I. The Effect of Fractional Derivatives on Thermo-Mechanical Interaction in Biological Tissues during Hyperthermia Treatment Using Eigenvalues Approach. *Fractal Fract.* **2023**, *7*, 432. https://doi.org/10.3390/fractalfract7060432

Academic Editors: Corina S Drapaca and Sameerah Jamal

Received: 3 May 2023
Revised: 20 May 2023
Accepted: 24 May 2023
Published: 26 May 2023

Copyright: © 2023 by the authors. Licensee MDPI, Basel, Switzerland. This article is an open access article distributed under the terms and conditions of the Creative Commons Attribution (CC BY) license (https://creativecommons.org/licenses/by/4.0/).

1. Introduction

The temperature behavior of living tissue is still not fully understood due to the difficulty in accurately measuring it in vivo. This is because necropsy can alter tissue temperature characteristics and examining tissue outside of the body lacks perfusion effects. Various in vivo techniques exist to measure thermal behavior, but they yield varying results, and precise measurement of tissue temperature in vivo remains elusive. For effective treatment, it is critical to control the body's heat transmission pathways. Thermal therapies aim to freeze or heat tumors without damaging surrounding healthy tissue. If doctors could predict how tissue would react thermally, they could plan therapy dosages and durations before surgery. Tissue and blood perfusion's temperature response is associated with a range of diseases and injuries, including diabetes, skin grafts, and frostbites. The severity of these diseases is influenced by the extent to which blood can reach a certain location. If the thermal characteristics of damaged tissue can be precisely monitored before problems arise, appropriate and efficient therapy can be provided immediately. Heat transport analysis in living tissue is challenging due to its diverse internal structure, which includes perfusion via capillary tubes, convection between blood and tissues, thermal conduction between solid tissues and blood arteries, and heating generation through metabolism, evaporation, and other factors. Pennes' [1] bioheat model, which is based on Fourier's law of thermal conduction, is used to represent heat transmission in living tissues. Various thermotherapy procedures, such as laser tissue welding [2], laser operations [3], and hyperthermia [4], are frequently utilized in modern medicine. Skin tissue temperature distributions are influenced by complex factors such as metabolic heating generation and

blood circulation, so researchers have expanded on basic relationships by incorporating a wide range of phenomenological mechanisms, such as metabolic heating production, thermal conduction, blood perfusions, radiation, and phase change. Biological tissues undergo diverse stages of change, which can take many different forms. Modified versions of Pennes' bioheat models, which employ various numerical methods, are available in the relevant literature. Several techniques have been used to study heat transmission in living tissues, including the homotopy perturbation technique [5], Legendre wavelets Galerkin approaches [6,7], and the finite element approach [8]. When a person's body temperature was unusually low, Esneault and Dillenseger [9] used finite difference approaches to investigate the time-dependent increase in temperature. During thermal therapy, Ghanmi and Abbas [10] performed an analytical investigation of the fractional time derivative in skin tissue. Marin et al. [11] utilized finite element analysis to study the nonlinear bio-heat model in skin tissue caused by external heating sources, while Hobiny and Abbas [12] explored the analytical solution for the fractional bioheat model in tissues with a spherical shape. On the other hand, Keangin and Phadungsak [13] conducted an analysis on the heat transport in porous liver during microwave ablation, specifically focusing on local thermal non-equilibrium. In their research, Keangin et al. [14] investigated the analysis of heat transfer in a deformed liver cancer model treated with a microwave coaxial antenna. Andreozzi et al. [15] studied the effects of a pulsating heat source on interstitial fluid transport in tumor tissues in which the effects of modulating-heat strategies to influence interstitial fluid transport in tissues were analyzed.

Different methods can be used to solve the time-dependent heat transfer equation and model infinite thermal propagations based on classical Fourier heat conduction. Fractional computation has recently proved to be a successful method for modifying many physical models. Fractional derivatives have received significant attention, and various definitions and methods have been developed. The use of fractional time derivatives has enabled the successful modification of many physical models' processes. Ezzat and colleagues introduced a novel bio-heat model based on the fractional heat conduction formulation, as described in their publications [16,17], while the investigation of transient heating in skin tissues caused by time-dependent thermal therapy, utilizing a heat transport law that incorporates memory, was carried out by Mondal and colleagues in reference [18]. Researchers have conducted several studies on the use of thermal transfer on living tissue [19] to improve treatment methods, develop more accurate temperature prediction technologies, and ultimately, find a cure for cancer. Over the past forty years, a wide range of researchers from various fields, including high-energy particle accelerators, continuum mechanics, acoustics, nuclear engineering, and aeronautics have expressed significant interest in generalized thermo-elastic models from both a technical and mathematical standpoint. The concepts of heat transfer and elasticity are linked in this model. Lord and Shulman [20] developed the thermo-elasticity hypothesis with multiple generalizations. Mondal et al. [21] employed the memory-dependent derivatives on a sliding interval within the framework of the Lord–Shulman model to investigate the heat transfer equation for this problem. Diaz et al. [22] used the finite element method to obtain the solutions of thermo-diffusion types present in living tissue to develop thermal damage. Zhu et al. [22] used the diffusion theory to consider rate process models for the results of thermal damages and the sedimentation of lighting energy in the tissue. When studying the actual phenomena of thermal transfer in finite media, the nonlinear and linear models of heating transfer are extended, and many authors have sought numerical or analytical solutions to the problems posed by these models [23–33]. Despite the growing popularity of laser, microwave, and other forms of thermal therapy in dermatology, thermo-mechanical interactions are seldom considered in current research, despite being central to the thermo-mechanically linked nature of these therapies. Generalized thermo-elastic models govern tissue thermo-elastic behaviors, which include the G-N model, the G-NII model, the DPL, the fractional model, and Li et al. [34–36], who further investigated the effects of heat-induced mechanical responses in skin tissues under temperature-dependent properties.

This research aims to create an analytical approach to examine the thermo-mechanical interactions with fractional time derivatives in living tissue that experiences instantaneous heating and has varying thermal and mechanical properties. A generalized thermo-elastic model is constructed that takes into account the tissue structure and variable thermal and mechanical characteristics within the bioheat transfer equation framework. The effect of fractional parameter in temperature, displacement, and thermal stress variations are shown in the graphics.

2. Materials and Methods

The field of bio-thermo-elasticity merges the principles of elasticity and bioheat conduction. The basic equations under fractional time derivatives in the living tissues can be given by [20,37,38]:

$$(\lambda+\mu)u_{j,ij}+\mu u_{i,jj}-\gamma T_{,i}=\rho\frac{\partial^2 u_i}{\partial t^2}, \tag{1}$$

$$k\nabla^2 T=\left(1+\frac{\tau_o^\beta}{\Gamma(\beta+1)}\frac{\partial^\beta}{\partial t^\beta}\right)\left(\rho c_e\frac{\partial T}{\partial t}+\omega_b\rho_b c_b(T-T_b)+\gamma T_o\frac{\partial^2 u}{\partial t\partial x}-Q_m\right), 0<\beta\leq 1, \tag{2}$$

$$\sigma_{ij}=\mu\left(u_{i,j}+u_{j,i}\right)+(\lambda u_{k,k}-\gamma(T-T_o))\delta_{ij}, \tag{3}$$

where t is the time, τ_o is the thermal relaxation time, T_b is the blood temperature, c_e refers to the specific heat at constant strain, ρ is the tissue mass density, $\gamma=(3\lambda+2\mu)\alpha_t$, α_t refers to the linear thermal expansion coefficient, λ, μ refer to the Lame's constants, T is the tissue temperature, k is the tissue thermal conductivity, ω_b is the blood perfusion rate, Q_m is the metabolic heat generation in skin tissues, e_{ij} are the strain components, σ_{ij} are the stress components, u_i are the displacement components, δ_{ij} is the Kronecker symbol and c_b is the blood specific heat. The definition of the fractional order derivative is as follows:

$$\frac{\partial^\beta h(\boldsymbol{r},t)}{\partial t^\beta}=\begin{cases} h(\boldsymbol{r},t)-h(\boldsymbol{r},0), & \beta\to 0,\\ I^{\beta-1}\frac{\partial h(\boldsymbol{r},t)}{\partial t}, & 0<\beta<1,,\\ \frac{\partial h(\boldsymbol{r},t)}{\partial t}, & \beta=1,\end{cases} \tag{4}$$

$$I^\nu h(\boldsymbol{r},t)=\int_0^t\frac{(t-s)^\nu}{\Gamma(\nu)}h(\boldsymbol{r},s)ds,\ \nu>0, \tag{5}$$

$$\lim_{\nu\to 1}\frac{\partial^\nu h(\boldsymbol{r},t)}{\partial t^\nu}=\frac{\partial h(\boldsymbol{r},t)}{\partial t}, \tag{6}$$

Equation (4) illustrates how the range of local thermal conduction can be characterized by two types of conductivity: standard thermal conduction and heat ballistic conduction. The fractional parameter is β, where $0<\beta\leq 1$ is used to define these conductivities. For normal conductivity, $\beta=1$, while for low conductivity $0<\beta<1$. Here, we assume that the surface and the bottom boundary of a limited domain of tissues with thickness L. As a result, the displacement components can be expressed as follows:

$$u_x=u(x,t), u_y=0, u_z=0. \tag{7}$$

So that the model has the following form

$$(\lambda+2\mu)\frac{\partial^2 u}{\partial x^2}-\gamma\frac{\partial T}{\partial x}=\rho\frac{\partial^2 u}{\partial t^2}, \tag{8}$$

$$k\frac{\partial^2 T}{\partial x^2}=\left(1+\frac{\tau_o^\beta}{\Gamma(\beta+1)}\frac{\partial^\beta}{\partial t^\beta}\right)\left(\rho c\frac{\partial T}{\partial t}+\omega_b\rho_b c_b(T-T_b)+\gamma T_o\frac{\partial^2 u}{\partial t\partial x}-Q_m\right), \tag{9}$$

$$\sigma_{xx}=(\lambda+2\mu)\frac{\partial u}{\partial x}-\gamma(T-T_o). \tag{10}$$

To obtain a solution for the equations, it is necessary to have two sets of initial and boundary conditions that align with the physical model description:

$$T(x,0) = T_b, \frac{\partial T(x,0)}{\partial t} = 0, u(x,0) = 0, \frac{\partial u(x,0)}{\partial t} = 0, \tag{11}$$

$$\sigma_{xx}(0,t) = 0,\ \sigma_{xx}(L,t) = 0, -k\frac{\partial T(x,t)}{\partial x}\bigg|_{x=0} = q_o\frac{t^2 e^{-\frac{t}{t_p}}}{16t_p^2}, -k\frac{\partial T(x,t)}{\partial x}\bigg|_{x=L} = 0, \tag{12}$$

where t_p points to the characteristic time of pulsing heat flux and q_o is constant. Now, the dimensionless quantities may be utilized for ease by employing:

$$T' = \frac{T - T_o}{T_o}, \left(t', \tau_o', t_p'\right) = \eta c^2\left(t, \tau_o, t_p\right),\ \left(x', u'\right) = \eta c(x,u),$$

$$\sigma_{xx}' = \frac{\sigma_{xx}}{\lambda + 2\mu},\ q_o' = \frac{q_o}{\eta c T_o K},\ Q_m' = \frac{Q_m}{T_o K \eta^2 c^2}, \tag{13}$$

where $\eta = \frac{\rho c_e}{K}$ and $c^2 = \frac{\lambda+2\mu}{\rho}$.

The primary equations can be expressed in a non-dimensional form by removing the dashes and introducing appropriate parameters, as shown in Equation (13):

$$\frac{\partial^2 u}{\partial x^2} - \varepsilon_1\frac{\partial T}{\partial x} = \frac{\partial^2 u}{\partial t^2}, \tag{14}$$

$$\frac{\partial^2 T}{\partial x^2} = \left(1 + \frac{\tau_o^\beta}{\Gamma(\beta+1)}\frac{\partial^\beta}{\partial t^\beta}\right)\left(\frac{\partial T}{\partial t} + \varepsilon_2 T + \varepsilon_3\frac{\partial^2 u}{\partial t \partial x} - Q_m\right), \tag{15}$$

$$\sigma_{xx} = \frac{\partial u}{\partial x} - \varepsilon_1 T, \tag{16}$$

$$u(x,0) = 0, \frac{\partial u(x,0)}{\partial t} = 0, T(x,0) = 0, \frac{\partial T(x,0)}{\partial t} = 0, \tag{17}$$

$$\sigma_{xx}(0,t) = 0, \sigma_{xx}(L,t) = 0, \frac{\partial T(x,t)}{\partial x}\bigg|_{x=0} = -q_o\frac{t^2 e^{-\frac{t}{t_p}}}{16t_p^2}, \frac{\partial T(x,t)}{\partial x}\bigg|_{x=L} = 0, \tag{18}$$

where $\varepsilon_1 = \frac{T_o\gamma_e}{(\lambda_e+2\mu_e)}, \varepsilon_2 = \frac{\rho_b c_b \omega_b}{K\eta^2 c^2}, \varepsilon_3 = \frac{\gamma_e}{\rho c_e}$.

3. Analytical Solutions in the Transform Domain

Equations (14)–(18) can be transformed using Laplace transforms, as in

$$\overline{f}(x,s) = L[f(x,t)] = \int_0^\infty f(x,t)e^{-st}dt. \tag{19}$$

Therefore, the following equations can be obtained

$$\frac{d^2\overline{u}}{dx^2} = s^2\overline{u} + \varepsilon_1\frac{d\overline{T}}{dx}, \tag{20}$$

$$\frac{d^2\overline{T}}{dx^2} = \left(1 + \frac{s^\beta\tau_o^\beta}{\Gamma(\beta+1)}\right)\left((s+\varepsilon_2)\overline{T} + s\varepsilon_3\frac{d\overline{u}}{dx}\right) - \frac{Q_m}{s}, \tag{21}$$

$$\overline{\sigma}_{xx} = \frac{d\overline{u}}{dx} - \varepsilon_1\overline{T}, \tag{22}$$

$$\overline{\sigma}_{xx}(0,s) = 0,\ \overline{\sigma}_{xx}(L,s) = 0, \frac{d\overline{T}(x,s)}{dx}\bigg|_{x=0} = \frac{-q_o t_p}{8\left(st_p+1\right)^3},\ \frac{d\overline{T}(x,s)}{dx}\bigg|_{x=L} = 0. \tag{23}$$

Equations (20) and (21) can be used to represent the vector–matrix differential equation as follows:

$$\frac{d\mathrm{M}}{dx} = BM - f, \tag{24}$$

where $M = \begin{pmatrix} \overline{u} \\ \overline{T} \\ \frac{d\overline{u}}{dx} \\ \frac{d\overline{T}}{dx} \end{pmatrix}$, $B = \begin{pmatrix} 0 & 0 & 1 & 0 \\ 0 & 0 & 0 & 1 \\ s^2 & 0 & 0 & \varepsilon_1 \\ 0 & \left(1 + \frac{s^\beta \tau_o^\beta}{\Gamma(\beta+1)}\right)(s+\varepsilon_2) & \left(1 + \frac{s^\beta \tau_o^\beta}{\Gamma(\beta+1)}\right)s\varepsilon_3 & 0 \end{pmatrix}$, $f = \begin{pmatrix} 0 \\ 0 \\ 0 \\ \frac{Q_m}{s} \end{pmatrix}$.

To solve Equation (24) using the eigenvalue techniques described in [39–48], Matrix B's characteristic equation is expressed as:

$$\alpha^4 - \left(s^2 + \left(1 + \frac{s^\beta \tau_o^\beta}{\Gamma(\beta+1)}\right)(s+\varepsilon_2) + \left(1 + \frac{s^\beta \tau_o^\beta}{\Gamma(\beta+1)}\right)s\varepsilon_3\varepsilon_1\right)\alpha^2 + \left(1 + \frac{s^\beta \tau_o^\beta}{\Gamma(\beta+1)}\right)(s+\varepsilon_2)s^2 = 0, \tag{25}$$

Relation (25) has four roots, which are the eigenvalues of matrix B, which are defined by $\pm\alpha_1$, $\pm\alpha_2$. The general solutions to the nonhomogeneous system (24) can be obtained by adding the complementary solution of the corresponding homogeneous system to a particular solution of the nonhomogeneous system. To find the particular solution to the nonhomogeneous Equation (24), we need to consider that the inhomogeneous terms in (24) contain functions of the Laplace parameter s. As a result, the particular solution can be expressed as:

$$\mathrm{M}(x,s) = A_1X_1e^{-\alpha_1 x} + A_2X_2e^{\alpha_1 x} + A_3X_3e^{-\alpha_2 x} + A_4X_4e^{\alpha_2 x} + \begin{pmatrix} 0 \\ R \\ 0 \\ 0 \end{pmatrix}. \tag{26}$$

where $R = \frac{Q_m}{s(s+\varepsilon_2)\left(1+\frac{s^\beta \tau_o^\beta}{\Gamma(\beta+1)}\right)}$. Hence, in the Laplace domain, the general solutions of displacement, temperature, and stress can be given by:

$$\overline{u}(x,s) = A_1U_1e^{-\alpha_1 x} + A_2U_2e^{\alpha_1 x} + A_3U_3e^{-\alpha_2 x} + A_4U_4e^{\alpha_2 x}. \tag{27}$$

$$\overline{T}(x,s) = A_1T_1e^{-\alpha_1 x} + A_2T_2e^{\alpha_1 x} + A_3T_3e^{-\alpha_2 x} + A_4T_4e^{\alpha_2 x} + R. \tag{28}$$

$$\overline{\sigma}_{xx} = A_1(-\alpha_1U_1 - \varepsilon_1T_1)e^{-\alpha_1 x} + A_2(\alpha_1U_2 - \varepsilon_1T_2)e^{\alpha_1 x} + A_3(-\alpha_2U_3 - \varepsilon_1T_3)e^{-\alpha_2 x} + A_4(\alpha_2U_4 - \varepsilon_1T_4)e^{\alpha_2 x} + R, \tag{29}$$

where U_i, T_i refer to the eigenvectors of displacement and temperature, respectively. The problem boundary conditions can be utilized to determine the values of A_1, A_2, A_3, and A_4. To obtain the final solutions for the displacement, temperature, and stress distributions, the Stehfest approach [49] can be used, which has an inverse function $f(x,t)$ defined by a specific formulation:

$$f(x,t) = \frac{ln2}{t}\sum_{j=1}^{M} V_j\overline{f}\left(x, j\frac{ln2}{t}\right), \tag{30}$$

where V_j can be given by

$$V_j = (-1)^{\frac{M}{2}+1}\sum_{k=\frac{i+1}{2}}^{min(i,\frac{M}{2})} \frac{k^{\frac{M}{2}+1}(2k)!}{\left(\frac{M}{2}-k\right)!k!(i-k)!(2k-1)!}$$

4. Numerical Outcomes and Discussion

To demonstrate the theoretical results discussed in the above sections, the numerical values of the physical parameters are presented. The material parameters for living tissues at the reference temperature, used in the following calculation, are denoted as follows [35]:

$$\lambda = 8.27 \times 10^8 (N)\left(m^{-2}\right), \alpha_t = 1 \times 10^{-4}\left(k^{-1}\right), T_o = 310(k),\ t_p = 0.15,$$

$$\mu = 3.446 \times 10^7 (N)\ \left(m^{-2}\right), c_b = 3770\ (J)\left(kg^{-1}\right)\left(k^{-1}\right),\ \rho_b = 1060(kg)\left(m^{-3}\right),$$

$$\tau_o = 0.05,\ K = 0.235\ (W)\left(m^{-1}\right)\left(k^{-1}\right),\ Q_m = 1.19 \times 10^3 (W)\left(m^{-3}\right),\ \rho = 1190(kg)\left(m^{-3}\right), c_e = 3600\ (J)\left(kg^{-1}\right)\left(k^{-1}\right)$$

The numerical values of the calculated physical quantities under the fractional biothermoelastic model, considering one thermal relaxation time and using the previous parameters, are displayed in Figures 1–12. Numerical calculations have been performed at time t = 0.2 to determine the temperature variations, the variation of displacement, and stress variation along the distance x under different values of the studied parameters as in Figures 1–12. Figures 1, 4, 7 and 10 display the temperature variation along the distance x. It can be observed from the figures that the temperature initially peaks at the tissue surface $(x = 0)$ due to the exponentially decaying pulse boundary heat flux. As the distance x increases, the temperature steadily decreases. Figures 2, 5, 8 and 11 display the variations of displacement along the distance x. Observing the figures, it can be noted that the displacement reaches its highest negative values at the tissue surface $(x = 0)$. Subsequently, it progressively increases towards peak values near the surface before decreasing back to zero. Figures 3, 6, 9 and 12 show the variation of stress σ_{xx} along the distance x. It can be observed that the stress σ_{xx} starts from zero and ends at zero to comply with the boundary condition of the problem. Figures 1–12 can be classified into four distinct groups.

In the first group, Figures 1–3 show the variations of temperature, displacement, and stress under various models. In Figures 1–3, the solid line (—) refers to the Pennes model (Pennes model) without thermal relaxation time ($\tau_o = 0$) and without fractional time derivative ($\beta = 1$), the dashed line (—) points to the single-phase lag model (SPL model) with one thermal relaxation time ($\tau_o = 0.02$) and without fractional time derivative ($\beta = 1$), while the dotted line (...) refers to the single-phase lag model under fractional time derivative (FSPL model) with one thermal relaxation time ($\tau_o = 0.02$) and with fractional time derivative ($\beta = 0.5$). The significant effects on the quantities under consideration are evident due to the various models.

In the second group, Figures 4–6 display the variation of temperature, displacement, and stress under different values of the fractional parameter ($\beta = 1, 0.5, 0.1$) when ($\tau_o = 0.02$). It is evident that the fractional time derivatives are responsible for the evident significant impacts on the quantities under consideration. A decrease in fractional time derivatives weakens the effect of thermo-mechanical propagation, as evidenced by a decrease in the maximum amplitude of temperature, displacement, and stress.

In the third group, Figures 7–9 show the variation of temperature, displacement, and stress under various values of thermal relaxation time ($\tau_o = 0,\ 0.02,\ 0.2$) under fractional time derivative when ($\beta = 0.5$). It is evident that the thermal relaxation time has significant effects on the quantities under consideration. The maximum amplitude of the temperature, displacement, and stress decreases with the increase the thermal relaxation time, which means that the thermal relaxation time is apt to weaken the effect of thermo-mechanical propagation.

In the fourth group, Figures 10–12 show the variations of temperature, displacement, and stress under various of the characteristic time of pulsing heat flux ($t_p = 0.1,\ 0.15,\ 0.2$) with one thermal relaxation time ($\tau_o = 0.02$) under fractional time derivative when ($\beta = 0.5$). It is observed that the characteristic time of pulsing heat flux has a significant effect on the

quantities under consideration. An increase in the characteristic time of pulsing heat flux weakens the effect of thermo-mechanical propagation, as evidenced by a decrease in the maximum amplitude of temperature, displacement, and stress.

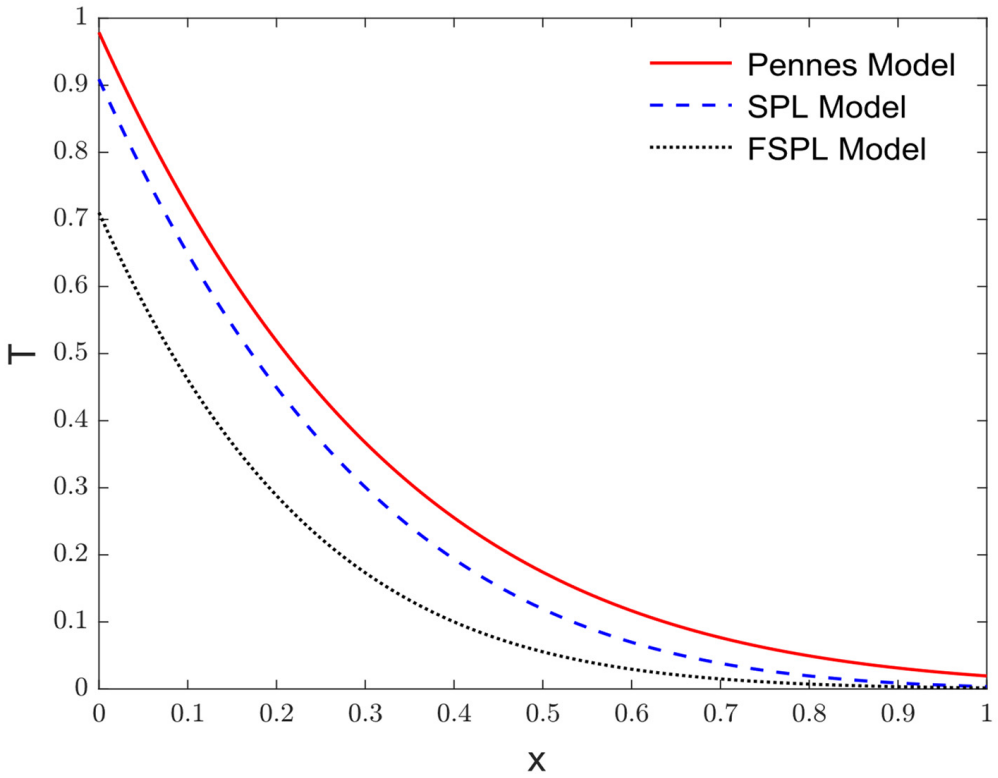

Figure 1. The temperature variations T via x under three different models.

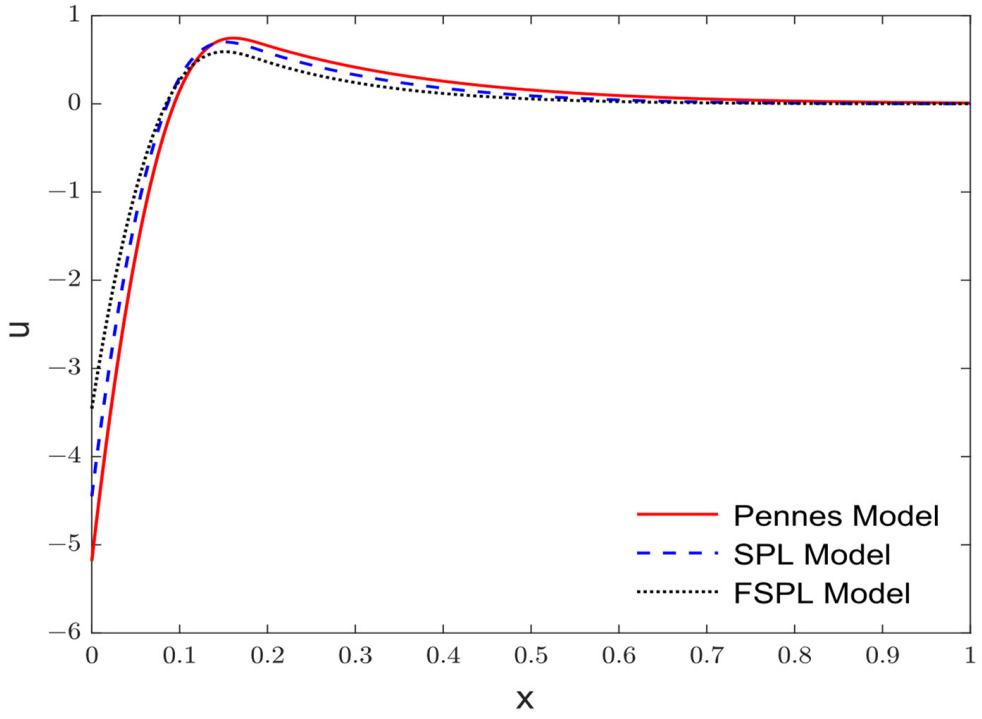

Figure 2. The variations of displacement u via x under three different models.

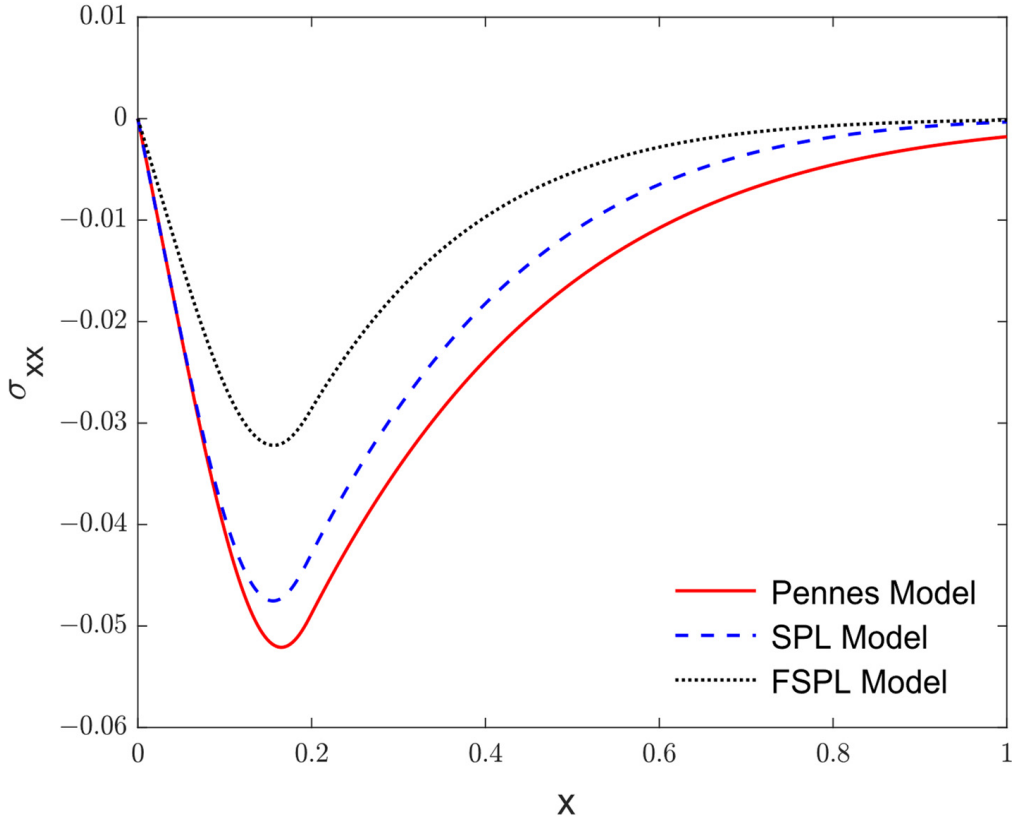

Figure 3. The variations of stress σ_{xx} via x under three different models.

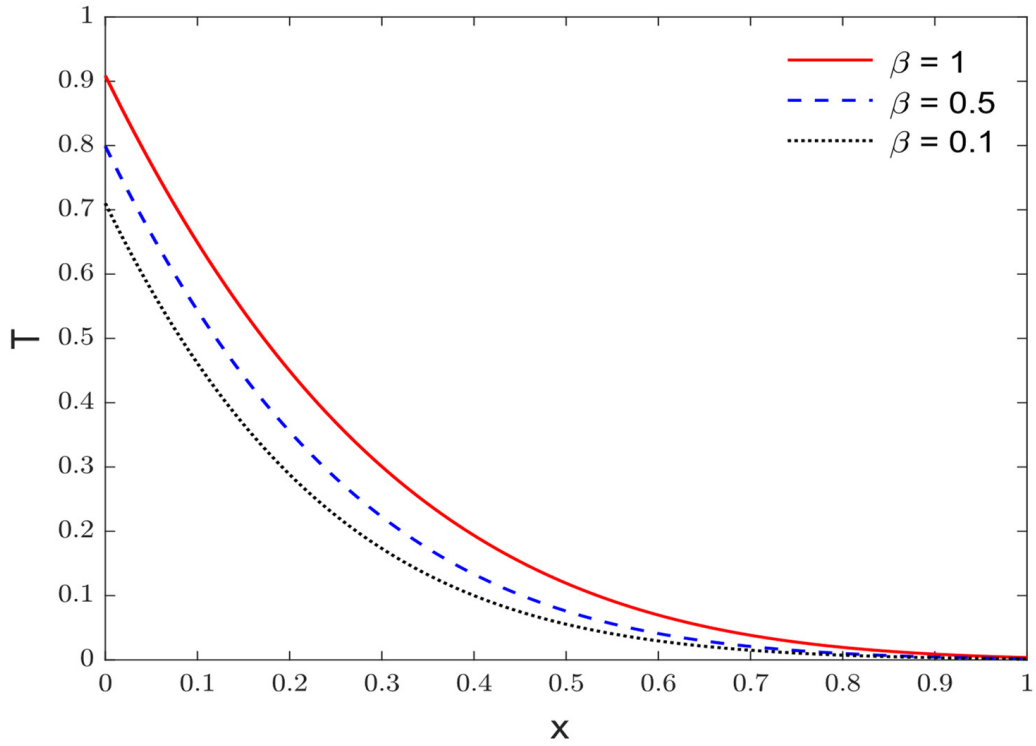

Figure 4. The temperature variations T via x under varying fractional parameter β.

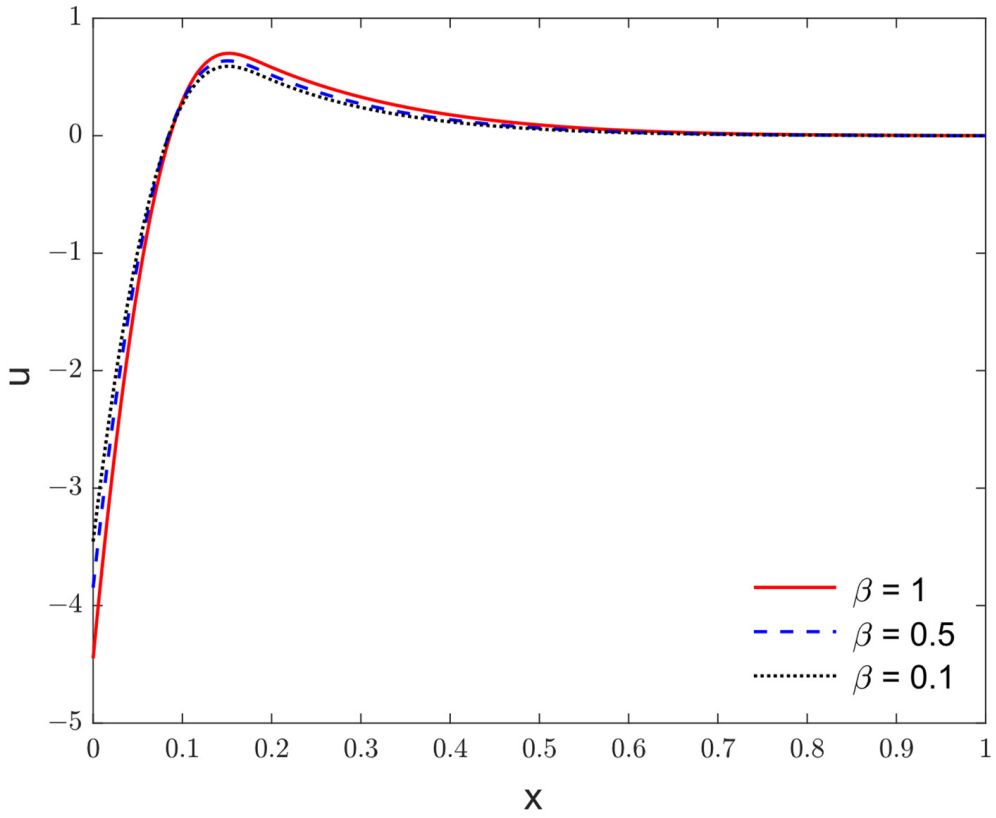

Figure 5. The variations of displacement u via x under varying fractional parameter β.

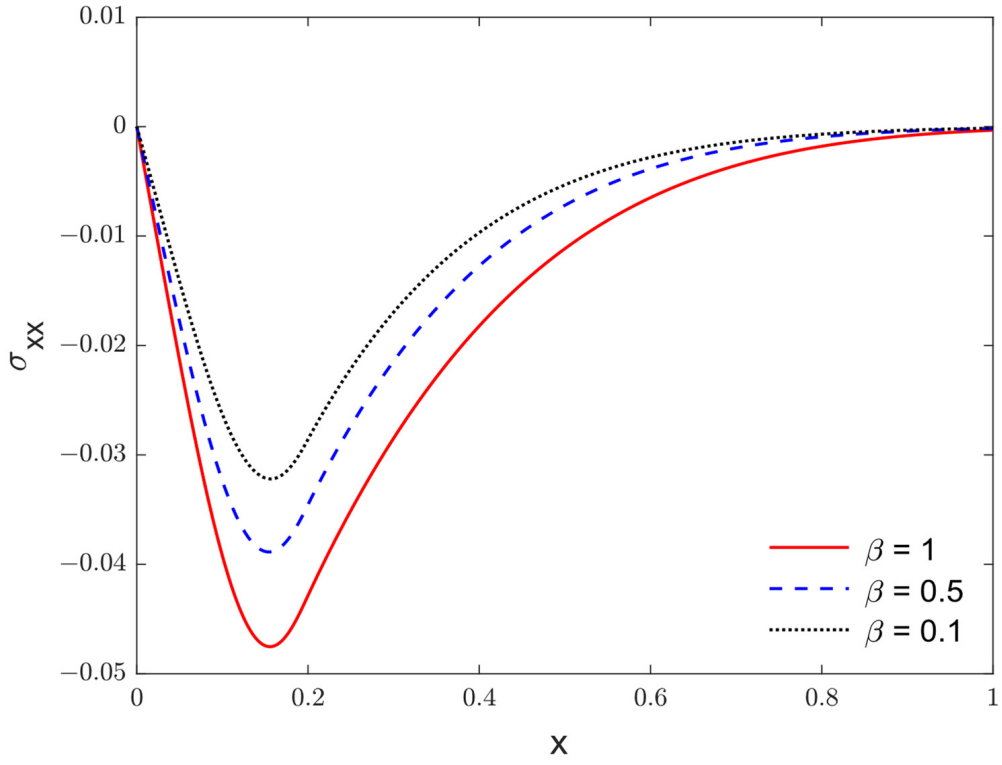

Figure 6. The variations of stress σ_{xx} via x under varying fractional parameter β.

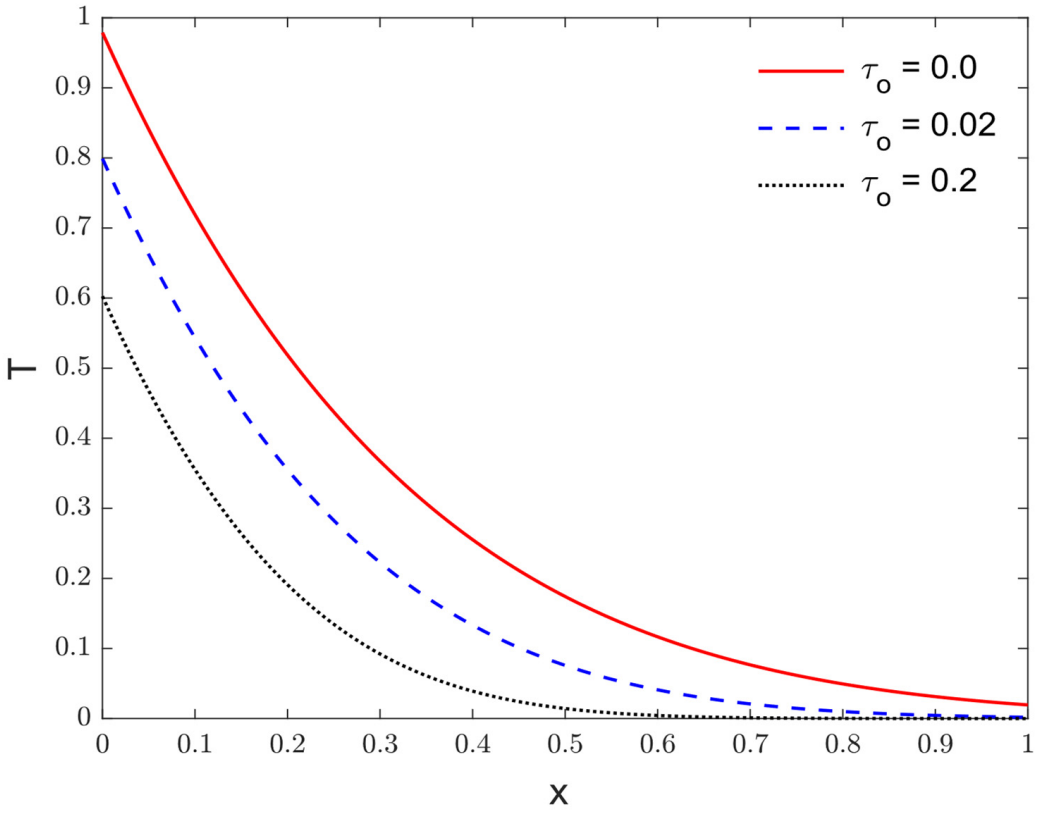

Figure 7. The temperature variations T via x under varying thermal relaxation time τ_o.

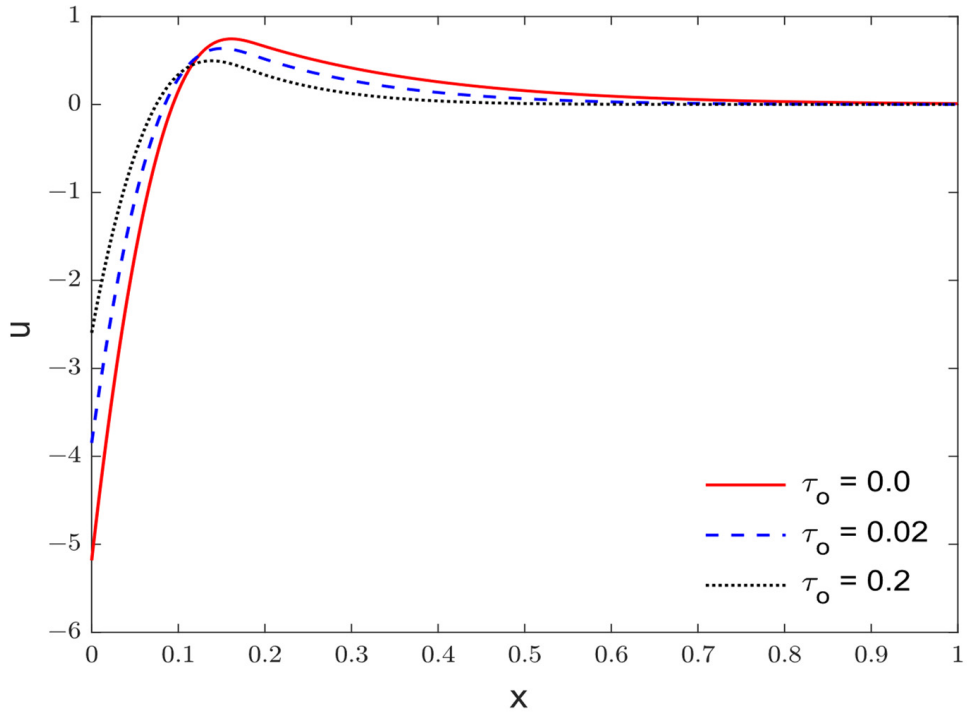

Figure 8. The variations of displacement u via x under varying thermal relaxation time τ_o.

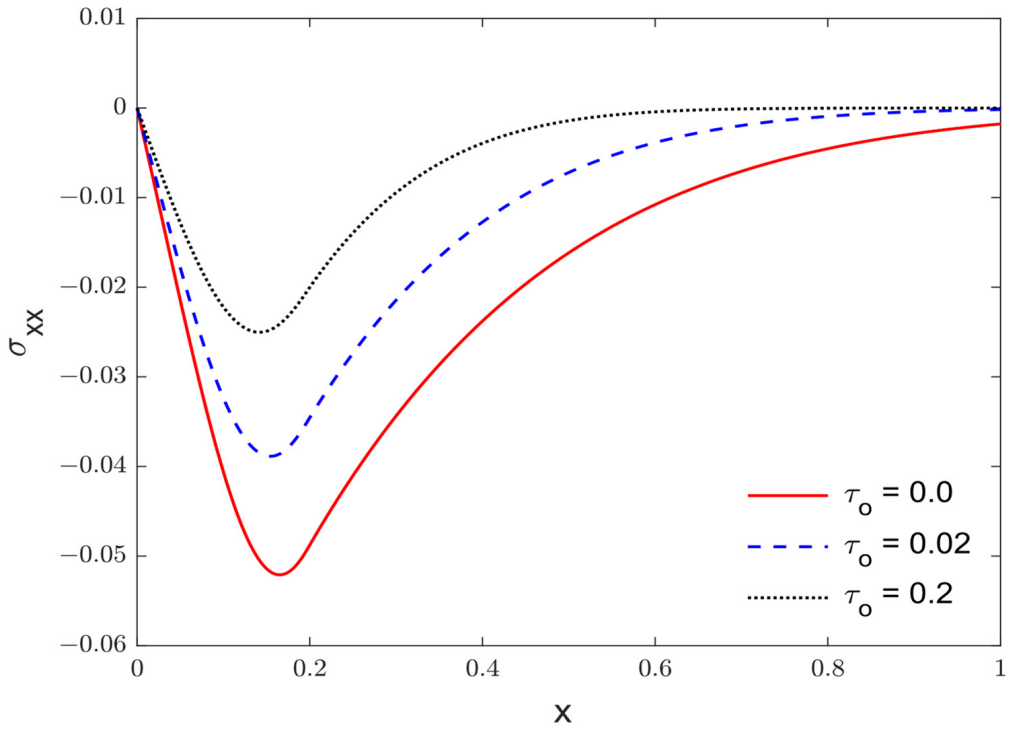

Figure 9. The variations of stress σ_{xx} via x under varying thermal relaxation time τ_o.

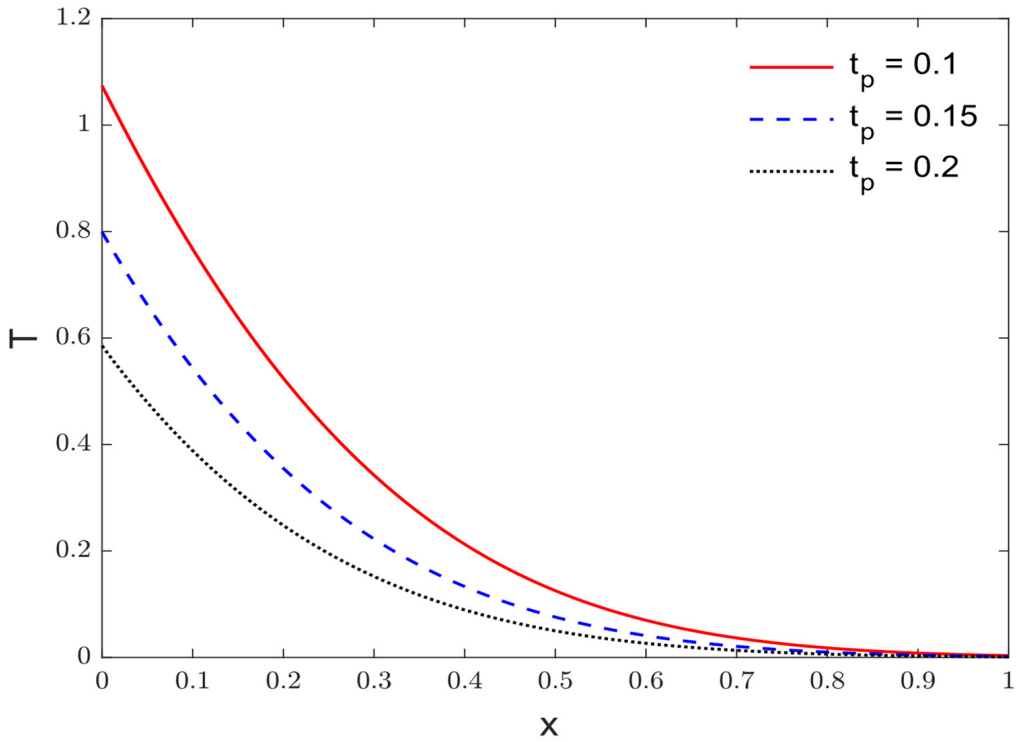

Figure 10. The temperature variations T via x under varying pulsing heat flux characteristic time t_p.

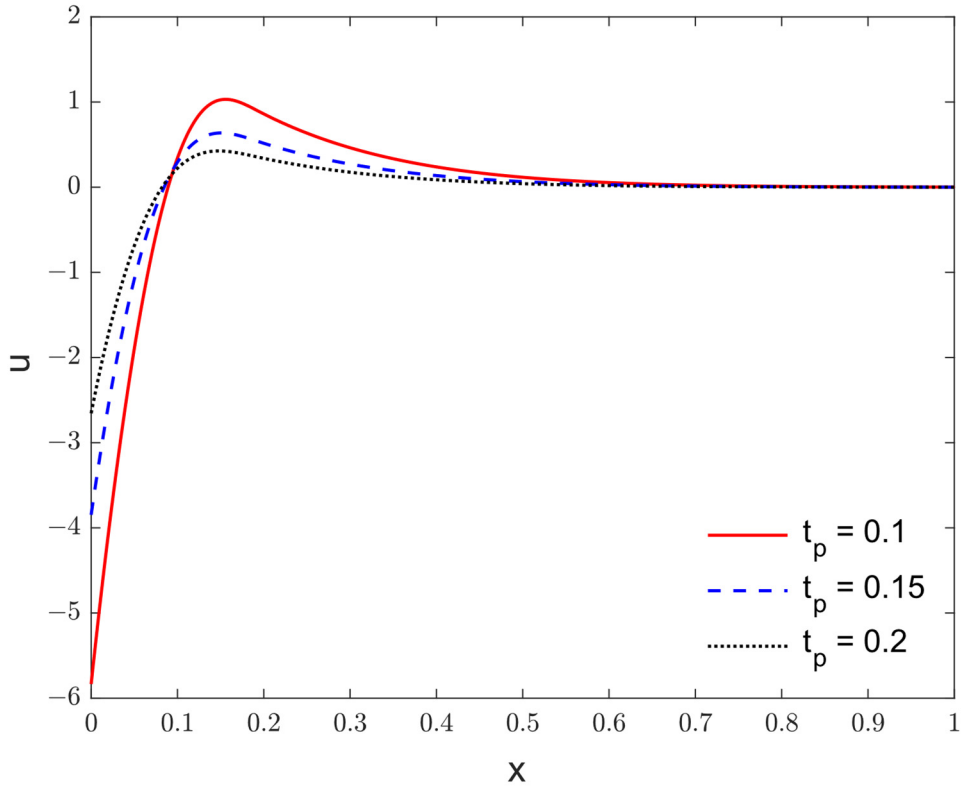

Figure 11. The variations of displacement u via x under varying pulsing heat flux characteristic time t_p.

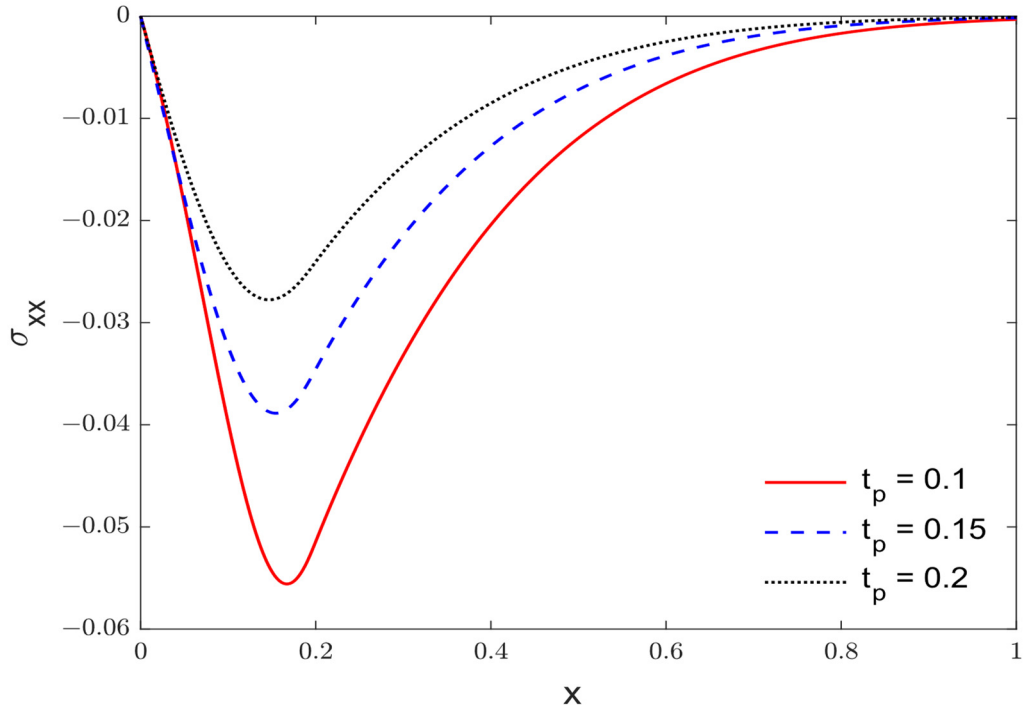

Figure 12. The variations of stress σ_{xx} via x under varying pulsing heat flux characteristic time t_p.

5. Conclusions

The aim of this research paper was to examine how biological tissues react to a sudden pulsing heat flux load by employing generalized thermo-elasticity under the fractional time derivatives framework, which incorporates one thermal relaxation time.

- This study specifically focused on the impacts of fractional parameter, thermal relaxation time, and the pulsing heat flux characteristic time on bio-thermo-elastic behaviors.
- A comparative analysis was conducted between the fractional single-phase lag model (FSPL model) and previous single-phase lag (SPL model) and Pennes (Pennes model) models.
- The findings of this study, which presented a modified thermo-elasticity approach, offered a fresh perspective on the propagation of thermal waves, representing the first attempts in this area.
- These results significantly contribute to enhancing our understanding of thermo-elastic behavior in living tissue.

Author Contributions: Conceptualization, A.H. and I.A.; methodology: A.H. and I.A.; validation: A.H. and I.A.; formal analysis: A.H. and I.A.; investigation: A.H. and I.A.; resources: I.A.; data curation: A.H. and I.A.; writing—original draft preparation: A.H. and I.A.; writing—review and editing: A.H.: visualization: I.A.; supervision: A.H. and I.A.; project administration: I.A. All authors have read and agreed to the published version of the manuscript.

Funding: This research work was funded by Institutional Fund Projects under grant no. (IFPIP: 93-130-1443). The authors gratefully acknowledge the technical and financial support provided by the Ministry of Education and King Abdulaziz University, DSR, Jeddah, Saudi Arabia.

Institutional Review Board Statement: Not applicable.

Informed Consent Statement: Not applicable.

Data Availability Statement: Not applicable.

Conflicts of Interest: The authors declare no conflict of interest.

References

1. Pennes, H.H. Analysis of tissue and arterial blood temperatures in the resting human forearm. *J. Appl. Physiol.* **1948**, *1*, 93–122. [CrossRef] [PubMed]
2. Gabay, I.; Abergel, A.; Vasilyev, T.; Rabi, Y.; Fliss, D.M.; Katzir, A. Temperature-controlled two-wavelength laser soldering of tissues. *Lasers Surg. Med.* **2011**, *43*, 907–913. [CrossRef] [PubMed]
3. Zhou, J.; Chen, J.; Zhang, Y. Dual-phase lag effects on thermal damage to biological tissues caused by laser irradiation. *Comput. Biol. Med.* **2009**, *39*, 286–293. [CrossRef] [PubMed]
4. Mahjoob, S.; Vafai, K. Analytical characterization of heat transport through biological media incorporating hyperthermia treatment. *Int. J. Heat Mass Transf.* **2009**, *52*, 1608–1618. [CrossRef]
5. Gupta, P.K.; Singh, J.; Rai, K. Numerical simulation for heat transfer in tissues during thermal therapy. *J. Therm. Biol.* **2010**, *35*, 295–301. [CrossRef]
6. Kumar, P.; Kumar, D.; Rai, K. A numerical study on dual-phase-lag model of bio-heat transfer during hyperthermia treatment. *J. Therm. Biol.* **2015**, *49*, 98–105. [CrossRef]
7. Yadav, S.; Kumar, D.; Rai, K.N. Finite Element Legendre Wavelet Galerkin Approch to Inward Solidification in Simple Body under Most Generalized Boundary Condition. *Z. Nat. A* **2014**, *69*, 501–510. [CrossRef]
8. Gupta, P.K.; Singh, J.; Rai, K.; Rai, S. Solution of the heat transfer problem in tissues during hyperthermia by finite difference–decomposition method. *Appl. Math. Comput.* **2013**, *219*, 6882–6892. [CrossRef]
9. Dillenseger, J.-L.; Esneault, S. Fast FFT-based bioheat transfer equation computation. *Comput. Biol. Med.* **2010**, *40*, 119–123. [CrossRef]
10. Ghanmi, A.; Abbas, I.A. An analytical study on the fractional transient heating within the skin tissue during the thermal therapy. *J. Therm. Biol.* **2019**, *82*, 229–233. [CrossRef]
11. Marin, M.; Hobiny, A.; Abbas, I. Finite element analysis of nonlinear bioheat model in skin tissue due to external thermal sources. *Mathematics* **2021**, *9*, 1459. [CrossRef]
12. Hobiny, A.; Abbas, I. Analytical solutions of fractional bioheat model in a spherical tissue. *Mech. Based Des. Struct. Mach.* **2021**, *49*, 430–439. [CrossRef]
13. Keangin, P.; Rattanadecho, P. Analysis of heat transport on local thermal non-equilibrium in porous liver during microwave ablation. *Int. J. Heat Mass Transf.* **2013**, *67*, 46–60. [CrossRef]
14. Keangin, P.; Wessapan, T.; Rattanadecho, P. Analysis of heat transfer in deformed liver cancer modeling treated using a microwave coaxial antenna. *Appl. Therm. Eng.* **2011**, *31*, 3243–3254. [CrossRef]

15. Andreozzi, A.; Iasiello, M.; Netti, P. Effects of pulsating heat source on interstitial fluid transport in tumour tissues. *J. R. Soc. Interface* **2020**, *17*, 20200612. [CrossRef]
16. Ezzat, M.A.; AlSowayan, N.S.; Al-Muhiameed, Z.I.; Ezzat, S.M. Fractional modelling of Pennes' bioheat transfer equation. *Heat Mass Transf.* **2014**, *50*, 907–914. [CrossRef]
17. Ezzat, M.A.; El-bary, A.A.; Al-sowayan, N.S. Tissue responses to fractional transient heating with sinusoidal heat flux condition on skin surface. *Anim. Sci. J.* **2016**, *87*, 1304–1311. [CrossRef]
18. Mondal, S.; Sur, A.; Kanoria, M. Transient heating within skin tissue due to time-dependent thermal therapy in the context of memory dependent heat transport law. *Mech. Based Des. Struct. Mach.* **2019**, *49*, 271–285. [CrossRef]
19. Andreozzi, A.; Brunese, L.; Iasiello, M.; Tucci, C.; Vanoli, G.P. Modeling Heat Transfer in Tumors: A Review of Thermal Therapies. *Ann. Biomed. Eng.* **2019**, *47*, 676–693. [CrossRef]
20. Lord, H.W.; Shulman, Y. A generalized dynamical theory of thermoelasticity. *J. Mech. Phys. Solids* **1967**, *15*, 299–309. [CrossRef]
21. Sur, A.; Mondal, S.; Kanoria, M. Influence of Moving Heat Source on Skin Tissue in the Context of Two-Temperature Caputo–Fabrizio Heat Transport Law. *J. Multiscale Model.* **2019**, *11*, 2050002. [CrossRef]
22. Díaz, S.H.; Nelson, J.S.; Wong, B.J. Rate process analysis of thermal damage in cartilage. *Phys. Med. Biol.* **2002**, *48*, 19. [CrossRef] [PubMed]
23. Ghazanfarian, J.; Saghatchi, R.; Patil, D. Implementation of Smoothed-Particle Hydrodynamics for non-linear Pennes' bioheat transfer equation. *Appl. Math. Comput.* **2015**, *259*, 21–31. [CrossRef]
24. Li, L.; Liang, M.; Yu, B.; Yang, S. Analysis of thermal conductivity in living biological tissue with vascular network and convection. *Int. J. Therm. Sci.* **2014**, *86*, 219–226. [CrossRef]
25. Selvi, C.; Srinivas, A.; Sreenadh, S. Peristaltic transport of a power-law fluid in an elastic tube. *J. Taibah Univ. Sci.* **2018**, *12*, 687–698. [CrossRef]
26. Khan, A.A.; Bukhari, S.R.; Marin, M.; Ellahi, R. Effects of chemical reaction on third-grade MHD fluid flow under the influence of heat and mass transfer with variable reactive index. *Heat Transf. Res.* **2019**, *50*, 1061–1080. [CrossRef]
27. Lata, P.; Himanshi. Orthotropic magneto-thermoelastic solid with higher order dual-phase-lag model in frequency domain. *Struct. Eng. Mech.* **2021**, *77*, 315–327. [CrossRef]
28. Abbas, I.A. A GN model for thermoelastic interaction in an unbounded fiber-reinforced anisotropic medium with a circular hole. *Appl. Math. Lett.* **2013**, *26*, 232–239. [CrossRef]
29. Abbas, I.A. Analytical solution for a free vibration of a thermoelastic hollow sphere. *Mech. Based Des. Struct. Mach.* **2015**, *43*, 265–276. [CrossRef]
30. Hobiny, A.; Abbas, I. A GN model on photothermal interactions in a two-dimensions semiconductor half space. *Results Phys.* **2019**, *15*, 102588. [CrossRef]
31. Marin, M.; Ellahi, R.; Vlase, S.; Bhatti, M. On the decay of exponential type for the solutions in a dipolar elastic body. *J. Taibah Univ. Sci.* **2020**, *14*, 534–540. [CrossRef]
32. Abo-Dahab, S.M.; Abouelregal, A.E.; Marin, M. Generalized thermoelastic functionally graded on a thin slim strip non-Gaussian laser beam. *Symmetry* **2020**, *12*, 1094. [CrossRef]
33. Alzahrani, F.; Hobiny, A.; Abbas, I.; Marin, M. An Eigenvalues Approach for a Two-Dimensional Porous Medium Based upon Weak, Normal and Strong Thermal Conductivities. *Symmetry* **2020**, *12*, 848. [CrossRef]
34. Li, X.; Li, C.; Xue, Z.; Tian, X. Analytical study of transient thermo-mechanical responses of dual-layer skin tissue with variable thermal material properties. *Int. J. Therm. Sci.* **2018**, *124*, 459–466. [CrossRef]
35. Li, X.; Xue, Z.; Tian, X. A modified fractional order generalized bio-thermoelastic theory with temperature-dependent thermal material properties. *Int. J. Therm. Sci.* **2018**, *132*, 249–256. [CrossRef]
36. Li, X.; Li, C.; Xue, Z.; Tian, X. Investigation of transient thermo-mechanical responses on the triple-layered skin tissue with temperature dependent blood perfusion rate. *Int. J. Therm. Sci.* **2019**, *139*, 339–349. [CrossRef]
37. Xu, F.; Seffen, K.; Lu, T. Non-Fourier analysis of skin biothermomechanics. *Int. J. Heat Mass Transf.* **2008**, *51*, 2237–2259. [CrossRef]
38. Ahmadikia, H.; Fazlali, R.; Moradi, A. Analytical solution of the parabolic and hyperbolic heat transfer equations with constant and transient heat flux conditions on skin tissue. *Int. Commun. Heat Mass Transf.* **2012**, *39*, 121–130. [CrossRef]
39. Abbas, I.A. Eigenvalue approach on fractional order theory of thermoelastic diffusion problem for an infinite elastic medium with a spherical cavity. *Appl. Math. Model.* **2015**, *39*, 6196–6206. [CrossRef]
40. Othman, M.I.A.; Abbas, I.A. Eigenvalue approach for generalized thermoelastic porous medium under the effect of thermal loading due to a laser pulse in DPL model. *Indian J. Phys.* **2019**, *93*, 1567–1578. [CrossRef]
41. Kumar, R.; Miglani, A.; Rani, R. Eigenvalue formulation to micropolar porous thermoelastic circular plate using dual phase lag model. *Multidiscip. Model. Mater. Struct.* **2017**, *13*, 347–362. [CrossRef]
42. Kumar, R.; Miglani, A.; Rani, R. Analysis of micropolar porous thermoelastic circular plate by eigenvalue approach. *Arch. Mech.* **2016**, *68*, 423–439.
43. Gupta, N.D.; Das, N.C. Eigenvalue approach to fractional order generalized thermoelasticity with line heat source in an infinite medium. *J. Therm. Stress.* **2016**, *39*, 977–990. [CrossRef]
44. Santra, S.; Lahiri, A.; Das, N.C. Eigenvalue Approach on Thermoelastic Interactions in an Infinite Elastic Solid with Voids. *J. Therm. Stress.* **2014**, *37*, 440–454. [CrossRef]

45. Baksi, A.; Roy, B.K.; Bera, R.K. Eigenvalue approach to study the effect of rotation and relaxation time in generalized magneto-thermo-viscoelastic medium in one dimension. *Math. Comput. Model.* **2006**, *44*, 1069–1079. [CrossRef]
46. Das, N.C.; Lahiri, A.; Giri, R.R. Eigenvalue approach to generalized thermoelasticity. *Indian J. Pure Appl. Math.* **1997**, *28*, 1573–1594.
47. Abbas, I.A.; Abdalla, A.-E.-N.N.; Alzahrani, F.S.; Spagnuolo, M. Wave propagation in a generalized thermoelastic plate using eigenvalue approach. *J. Therm. Stress.* **2016**, *39*, 1367–1377. [CrossRef]
48. Abbas, I.; Hobiny, A.; Marin, M. Photo-thermal interactions in a semi-conductor material with cylindrical cavities and variable thermal conductivity. *J. Taibah Univ. Sci.* **2020**, *14*, 1369–1376. [CrossRef]
49. Stehfest, H. Algorithm 368: Numerical inversion of Laplace transforms [D5]. *Commun. ACM* **1970**, *13*, 47–49. [CrossRef]

Disclaimer/Publisher's Note: The statements, opinions and data contained in all publications are solely those of the individual author(s) and contributor(s) and not of MDPI and/or the editor(s). MDPI and/or the editor(s) disclaim responsibility for any injury to people or property resulting from any ideas, methods, instructions or products referred to in the content.